

# Slurry Erosion Performance of High-Velocity Flame-Sprayed Ni-20Al<sub>2</sub>O<sub>3</sub> and Ni-10Al<sub>2</sub>O<sub>3</sub>-10TiO<sub>2</sub> Coatings Under Accelerated Conditions

Rajeev Kumar<sup>1</sup> · Sanjeev Bhandari<sup>2</sup> · Atul Goyal<sup>3</sup>

Submitted: 28 February 2017 / in revised form: 24 June 2017 / Published online: 17 July 2017  
© ASM International 2017

**Abstract** The slurry erosion wear behavior of Ni-20Al<sub>2</sub>O<sub>3</sub> and Ni-10Al<sub>2</sub>O<sub>3</sub>-10TiO<sub>2</sub> coatings, deposited by high-velocity flame-sprayed technique, has been evaluated in the present investigation. A series of slurry erosion tests were conducted on the deposited surfaces, using an indigenously developed slurry erosion test rig under varying environmental conditions. The effect of identifying operational parameters like rotational speed, average particle size of erodent and erodent concentration on erosion behavior was also evaluated. Surface roughness tester, scanning electron microscope and XRD apparatus were utilized as surface characterization tools, whereas Vickers's microhardness tester and bond strength tester were employed for mechanical analysis. The SEM observations of eroded specimens were observed to be lying in close proximity to the reported experimental results. Irrespective of the test conditions, Ni-10Al<sub>2</sub>O<sub>3</sub>-10TiO<sub>2</sub> coating showed better results of slurry erosion performance in comparison with Ni-20Al<sub>2</sub>O<sub>3</sub> coating. Further, each operational test parameter revealed a proportional effect on the erosion rate of both the coatings.

**Keywords** alumina-titania · erodent · HVFS · nickel-alumina · nickel-alumina-titania · specific mass loss

## Introduction

Many hydropower projects, especially in the Himalayan and northeastern regions of India, regularly faces slurry erosion problems in turbines, which directly affects the overall efficiency of power generation units (Ref 1). The problem becomes highly complex during the monsoon days due to the sudden increase in solid (especially quartz) concentration levels (Ref 2). However, sometimes, it is better to shut down the hydro-plants to prevent the major losses. Normally, the decision of shutting down the whole plant is taken when the solid content exceeds the threshold value (usually 5% of sand) of solid concentration (Ref 3). The turbine components vulnerable to slurry erosion are buckets, impellers, nozzles, spear and needles, in the case of impulse turbines, and guide vanes, impeller blades, faceplate and labyrinth seal, in the case of reaction turbines (Ref 4).

Martensitic stainless steel, CA6NM (13/4), is commonly used for the manufacturing of some of the hydro-turbine components. Among the other structural steel grades, such as CF8M, 16Cr5Ni and 13Cr1Ni, CA6NM (13/4) remains a preferred choice due to its high impact strength and fracture toughness properties (Ref 5). However, during the long duration of exposure to slurry impacts, this steel undergoes significant degradation due to their lower value of hardness (310 HV) in comparison with the erodent particles having more than 1100 HV hardness value. This could result in poor slurry erosion performance of CA6NM material (Ref 6). To overcome this limitation, various attempts have been tried such as the development of high resistance materials, application of surface coatings, improvement in the design of components and minimizing the erodent contents in the water. Among these options, surface coatings, especially thermal spray coatings, appear to be most viable one in order to enhance the life span of the components. Extensive

✉ Sanjeev Bhandari  
sanjeev.bhandari@bbsbec.ac.in

<sup>1</sup> IKGPTU – Research Scholar, Mechanical Engineering, Jalandhar, India

<sup>2</sup> Baba Banda Singh Bahadur Engineering College, Fatehgarh Sahib, Fatehgarh Sahib, India

<sup>3</sup> Lala Lajpat Rai Institute of Engineering and Technology, Moga, Punjab, India

studies addressing the improvement in slurry erosion response of materials by the application of various thermal spray techniques have been presented earlier. Further, the evolution of high-velocity flame spray (HVFS) process provided homogeneous and highly dense coatings with lesser number of pores than those from other thermal spray processes. This process is also featured with low cost of the spraying system (Ref 7). Grewal et al. (Ref 7) utilized the HVFS process for the deposition of Ni-Al<sub>2</sub>O<sub>3</sub> coatings and reported the development of porous free coating, which results in improved mechanical properties as well as slurry erosion resistance. They also suggested that the proportion of reinforcement and matrix phase highly contributes to the mechanical performance of the coating system.

A quantum of studies had already been carried out by a number of researchers in the field of exploring the potential of various coating combinations. Due to the optimum combination of hardness and toughness properties, the WC-based coatings, especially WC-Co-Cr coatings, are mainly preferred for the applications owing to slurry erosion. However, the high cost incurred with these coatings limits their acceptability for general applications (Ref 8–10). It becomes thus essential to explore the capabilities of other cheaper alternatives in order to meet the demand of high service components. The Ni-Al<sub>2</sub>O<sub>3</sub> coating combination is one of the alternatives that prove to be having significant slurry erosion resistance (Ref 11). Further, the use of Al<sub>2</sub>O<sub>3</sub>-TiO<sub>2</sub> coatings as a slurry erosion resistance material has a long history. High fracture toughness, low thermal conductivity and thermal expansion are some of the important features of this coating combination. Moreover, the content of titania, in general, is found to be highly contributing toward enhancing the mechanical properties as well as wear resistance of Al<sub>2</sub>O<sub>3</sub> coatings (Ref 12). In the view of the above aspects, the two coating combinations, viz. Ni-Al<sub>2</sub>O<sub>3</sub> and Ni-10Al<sub>2</sub>O<sub>3</sub>-10TiO<sub>2</sub>, have been investigated in the present study. Further, these coatings were deposited onto the target material by utilizing HVFS system. The lower cost of the spraying system along with low cost of deposit coating material could provide a better alternative to the high-cost incurred coating systems.

The process of slurry erosion is generally considered as the gradual removal of surface material caused by repeated deformation as well as cutting actions (Ref 13). The slurry erosion is a complex phenomenon, as it is influenced by a number of factors, which act simultaneously (Ref 14). Among all the factors, impingement angle, composition of the slurry, average size of the erodents, slurry concentration and impact velocity factors were reported as the most significant factors those highly contribute to slurry erosion (Ref 15). However, these factors are found to so intertwine that analyzing the effect of a single variable even in laboratory scale becomes highly cumbersome (Ref 16). Some

studies have endeavored in the field of developing a correlation between slurry erosion response and influential parameters (Ref 17–19). The erosion rate can be determined by using the following relation (Ref 17):

$$E_w = KV^\alpha d^\beta C^\gamma \quad (\text{Eq 1})$$

where  $E_w$ ,  $V$ ,  $d$  and  $C$  are designated for erosion rate, velocity, erodent size and slurry/erodent concentration, respectively, whereas  $K$ ,  $\alpha$ ,  $\beta$ ,  $\gamma$  are designated for various constants whose magnitudes depend on the target material and erodent properties.

It has been learned from the literature that the fundamental understanding of erosion behavior is necessary in order to mitigate the effects of the slurry erosion process. The present investigation provides novel insight on the comparative slurry erosion performance of HVFS deposited Ni-20Al<sub>2</sub>O<sub>3</sub> and Ni-10Al<sub>2</sub>O<sub>3</sub>-10TiO<sub>2</sub> coatings under various environmental conditions. To achieve this objective, the coated specimens were subjected to an indigenously developed high-speed slurry erosion test rig. The test rig was developed, as standardized test rig available with the authors (Model: TR401, DUCOM, Bangalore, India) exhibited some limitations such as interrupted slurry flow throughout the flow circuit and inadequate erosive suspension in the water media. Due to the involvement of these factors, the data generated may have limited application for quantitative analysis. Better control over slurry flow, improved slurry suspension and simultaneous testing of six specimens are some of the features associated with the developed test rig. Through the utilization of indigenously developed slurry erosion test rig, the results established the material loss of each coating under various test conditions and allowed conclusions to be drawn concerning the influence of testing conditions on the respective erosion performance of the test coatings. Mechanical analysis, as well as surface characterization, facilitated the evaluation of coating properties and assessment of damage within the impact region. This body of research seeks to develop an enhanced understanding of the erosion performance of HVFS deposited Ni-Al<sub>2</sub>O<sub>3</sub> and Ni-Al<sub>2</sub>O<sub>3</sub>-TiO<sub>2</sub> coatings.

## Experimental Details

### Materials and Methods

Martensitic steel having grade CA6NM, commonly used for manufacturing of various parts of a hydro-turbine system, was utilized as a substrate in the present investigation. The steel ingots in the form of square cross-sectional bars (1000 × 15 × 15 mm<sup>3</sup>) were procured from Mithila Malleables Pvt. Ltd., India. The nominal composition of the

steel is as follows: 0.058 C<sub>Max.</sub>, 0.664 Si<sub>Max.</sub>, 0.493 Mn<sub>Max.</sub>, 0.026 P<sub>Max.</sub>, 11.56 Cr<sub>Max.</sub>, 0.017 S<sub>Max.</sub>, 3.62 Ni<sub>Max.</sub>, 0.493 Mo<sub>Max.</sub> and Fe as balance. Some of the mechanical properties of CA6NM steel (Ref 20) are listed in Table 1. For the slurry tests, the cylindrical specimens having dimensions of outer diameter 12 mm, inner diameter 6 mm and height 10 mm were prepared from the as-obtained steel ingot.

The high-velocity flame spray (HVFS) system, which is a proprietary product of Metallizing Equipments Company Pvt. Ltd. (MECPL), Jodhpur, India, was employed for the development of the coatings. Prior to the deposition of coatings, the surface of each specimen was activated by grit blasting using alumina particles. The commercially available Ni, Al<sub>2</sub>O<sub>3</sub> and TiO<sub>2</sub> powders were used to prepare the required proportions of feedstock powders. Some of the physical properties of individual powders are presented in Table 2, whereas the XRD patterns of these powders are depicted in Fig. 1. The XRD results confirm the presence of desired phases. Table 3 exhibits the detail of HVFS process parameters during the deposition process. As per the recommendation provided by the technical experts of Metallizing Equipments Company Pvt. Ltd. (MECPL), Jodhpur, India, the deposition of both the feedstock powders was done using same process parameters. During the spraying process, the surface temperature of in-flight particles was measured by using Spray Watch (Model: Spray Watch 2i, Osier, Finland). The designation system employed for the developed coatings is given in Table 4. The sand used for the slurry tests was collected from near to Nathpa Jakhri Dam, H.P., India. The sieve analysis (Fig. 2) of the collected sand was done to obtain the different grain-size sand particles. Thereafter, a standardized sieving procedure (Ref 21, 22) was adopted for preparing the required average-size sand samples (300 and 500 μm). The detail for the preparation of required sand samples is given in Table 5. To calculate the average size, each sieve has been given a weightage factor known as multiplier, whose value is same as the number of the preceding sieve. The amount retained on each sieve is multiplied by the respective multiplier, summed up and then divided by the

total mass of the sample giving the average fineness number. The same can be expressed as:

$$AFN = \frac{\sum M_i W_i}{\sum W_i} \tag{Eq 2}$$

The mesh size corresponds to the determined value of AFN giving the average particle size of prepared sand sample.

### Experimental Setup and Instrumentation

A closed-loop slurry erosion test rig was indigenously developed to conduct the various slurry erosion experiments. The tester (Fig. 3) is composed of a rotor assembly, solid-liquid mixing tank, a mud pump, abrasion chamber, variable speed D.C. motor and a stirrer. The stainless steel material was used to fabricate the rotor assembly, slurry tank and abrasion chamber. The rotor assembly includes a vertical shaft, whose one end was permanently fixed to a circular disk, whereas the other was attached to a belt pulley arrangement for the power driven purpose. During the slurry testing, the specimens were carefully mounted onto the circular disk at specific locations (symmetrically spaced holding pins). The most important feature of the test rig is that it can test six specimens simultaneously. This feature has eliminated the chance of errors during experimentation, as each specimen was exposed under identical environmental conditions. The slurry tank is rectangular in shape with 30 liters of slurry mixture holding capacity. Mud pump was used to attain the regular flow of slurry media within the flow circuit. The abrasion chamber is a closed vessel of five liters capacity, wherein the slurry media interact with the testing surfaces. A stirrer/agitator was also incorporated in the present tester to improve the slurry suspension within the slurry tank. The slurry erosion testing was performed in accordance with the procedure given in ASTM standard G-73. During the single test, the test specimens were operated for a total duration of 6 h, whereas the test was interrupted after a regular interval of 1 h for mass loss measurements. Prior

**Table 1** Mechanical properties of CA6NM material (Ref 20)

Material and grade	Brinell hardness, HBW	Tensile strength, MPa	Yield strength, MPa
CA6NM (13Cr/4Ni)	269	755	550

**Table 2** Detail of the powders used in the present investigation

Powder	Make	Morphology	Particle shape	Particle size, μm
Nickel (Ni)	Amperit, H.C. Starck	Water atomized	Spherical	20-100
Alumina (Al <sub>2</sub> O <sub>3</sub> )	Amperit, H.C. Starck	Fused and crushed	Irregular	20-60
Titania (TiO <sub>2</sub> )	Amperit, H.C. Starck	Fused and crushed	Blocky type	15-45

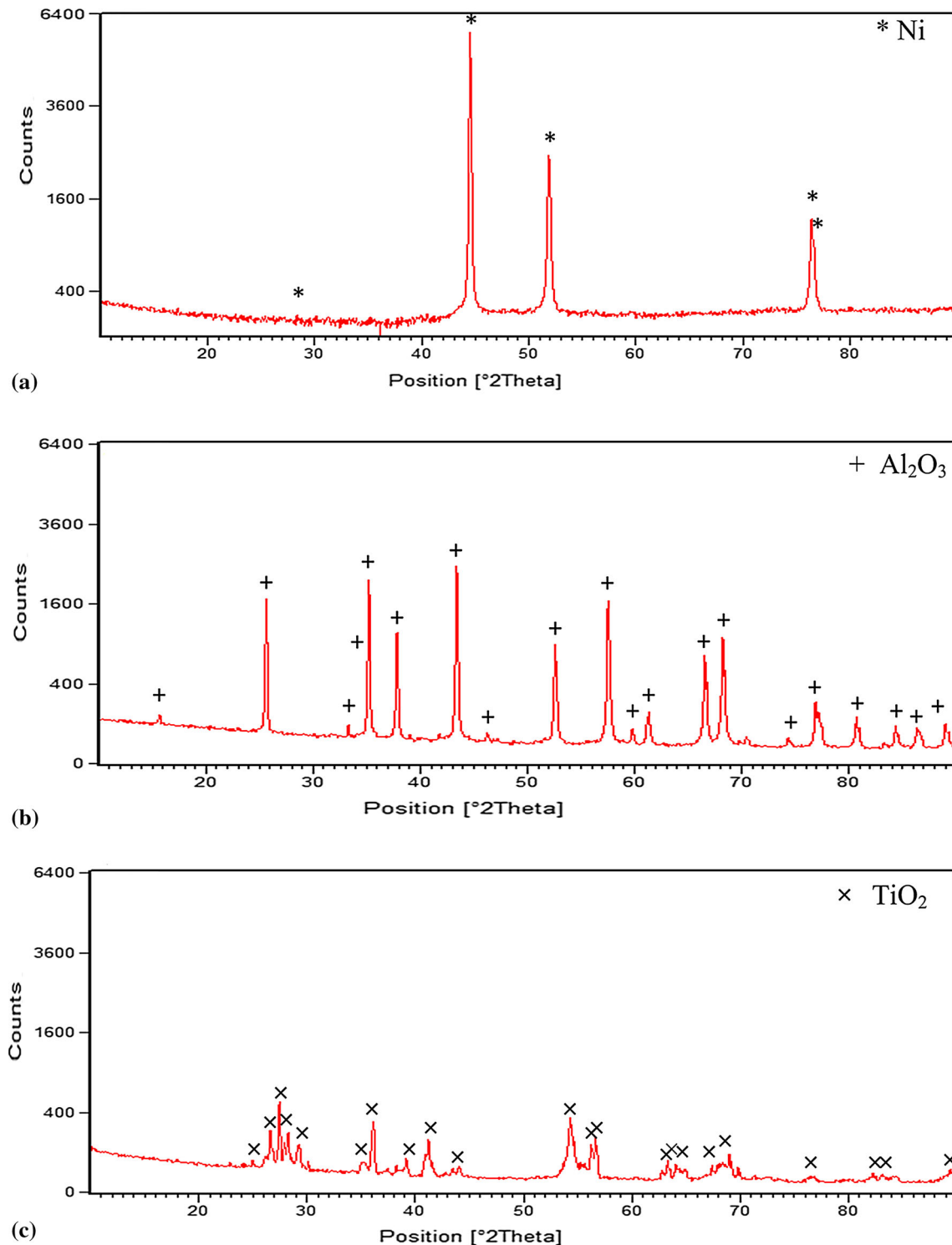


**Fig. 1** XRD analysis of powders used for preparing required deposits

to this, each test specimen was properly washed using acetone and then dried under hot air blow. The mass measurements were taken with the help of a precise digital microbalancer having least count of 0.0001 g.

### Parameters Investigated and Experimental Plan

The present study is aimed at investigating the variations in three important parameters, viz. rotational speed, average particle size of erodent and erodent concentration, on the

slurry erosion rate of developed coatings. For this objective, two ranges of each test parameter were selected and are presented in Table 6. Further, these parameters were optimized using Taguchi’s L4 methodology. The parameters and their values used to conduct the experiments are listed in Table 7.

**Microstructural and Mechanical Characterization**

The contact-type surface roughness tester (Mitutoyo, Model: Surftest SJ 301), scanning electron microscope

**Table 3** HVFS process parameters used for deposition process

Parameter	Value
Particle temperature, °C	2600
Oxygen flow rate, lpm	40
Acetylene flow rate, lpm	65
Powder feed rate, g/min	10
Air pressure, kg/cm <sup>2</sup>	3.5
Spraying distance, mm	20

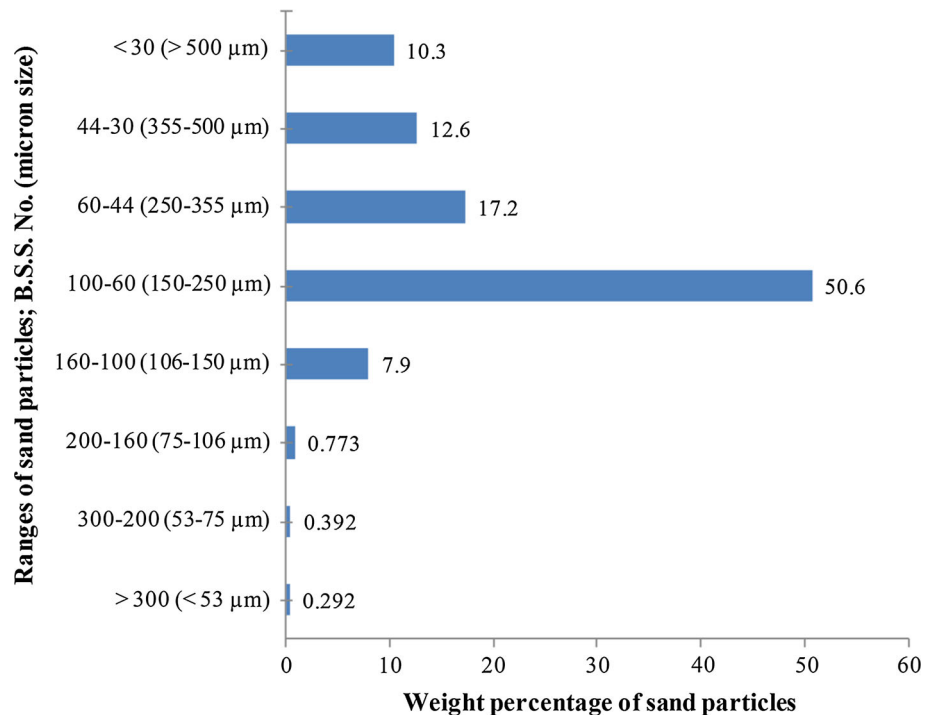
**Table 4** Designation system used for the developed coatings

Designation	Elements		
	Nickel, %	Alumina, %	Titania, %
Ni-A	80	20	...
Ni-AT	80	10	10

(JEOL; Model: JSM-6510LV) and XRD apparatus (PANalytical, Model: X’Pert Pro) were utilized as surface characterization tools in the present investigation. A tracing length of 6 mm was decided for the surface roughness measurements. Ten test replicates of each surface were carried out to provide an average surface roughness value. For cross-sectional examination, the as-sprayed samples were cross-sectioned by means of a slow-speed diamond cutter followed by mounting in epoxy using hot mounting press. These mounted samples were then ground down to 1500 grit using emery papers. Further, the grounded samples were polished with the help of cloth-wheel polishing machine using alumina as a slurry powder. The SEM micrographs allowed evaluation of the wear scar regions and helped in analyzing the various mechanisms responsible for material removal. XRD measurements were taken over a scanned range ( $2\theta$  range) of 20°-90°.

The mechanical tests were performed to confirm the soundness of the developed coatings. A Vickers microhardness tester (Model: SHV-1000, Chennai Metco Private Limited, Chennai, India) was employed for measuring hardness by conducting Vickers indentation at a loading force of 300 g and dwell time of 30 s. Ten readings of each measurement for each surface were made to determine the average value of microhardness. A tensile adhesion test in accordance with ASTM-C633 was performed for bond strength measurements (Ref 23). In this test, the two identical-sized (a cylinder  $\varnothing$  25.4 mm  $\times$  25.4 mm long) specimens, one coated and other uncoated were glued to each other using an epoxy adhesive (HTK Ultra-bond 100). The

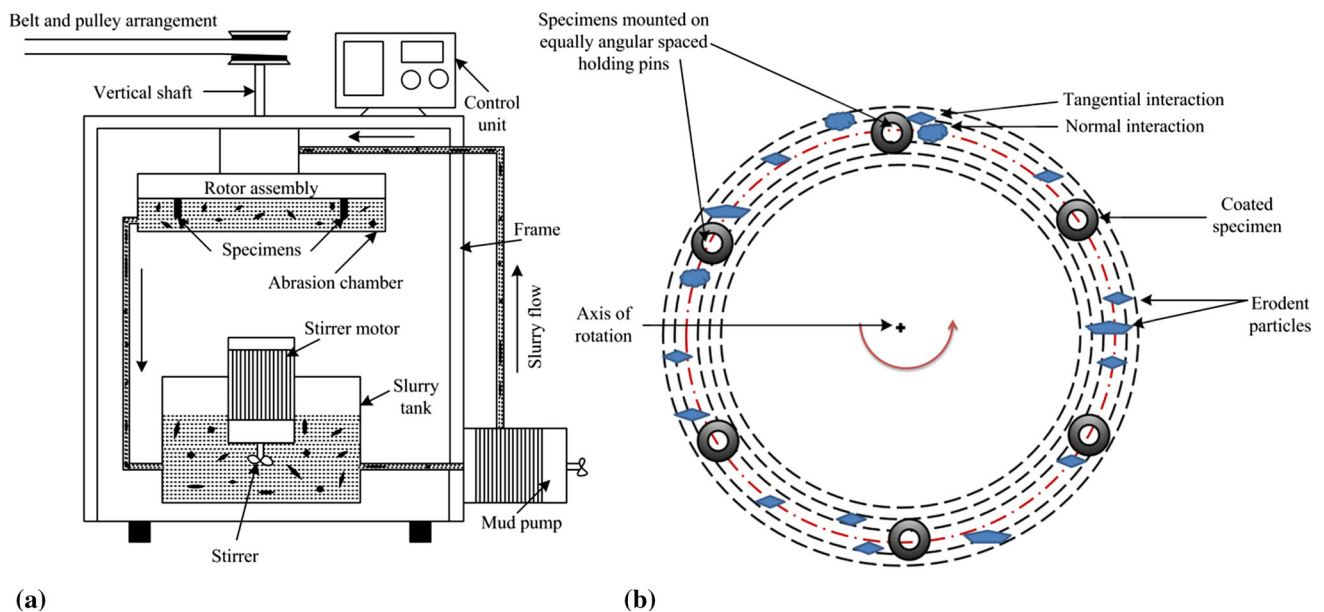
**Fig. 2** Sieve analysis [particle size distribution (PSD)] of collected sand



**Table 5** Preparation of 300 and 500  $\mu\text{m}$  sand samples

B.S.S. no.	Multiplier ( $M_i$ )	Weight used, g ( $W_i$ )	Multiplier(a) wt. used ( $M_iW_i$ )	Weight used, g ( $W_i$ )	Multiplier(a) wt. used ( $M_iW_i$ )
30	20	400	8000	700	14,000
44	30	200	6000	640	19,200
60	44	200	8800	400	17,600
100	60	40	2400	200	12,000
160	100	40	4000	30	3000
200	160	40	6400	30	4800
300	200	40	8000	...	...
>300	300	40	12,000	...	...
Total wt. = 1000 (g)			Total = 55,600	Total wt. = 2000 (g)	Total = 70,600
AFN = 55,600/1000 = 55.6				AFN = 70,600/2000 = 35.3	
BSS No. 55.6 $\approx$ 300 $\mu\text{m}$				BSS No. 35.3 $\approx$ 500 $\mu\text{m}$	

AFN average grain fineness number

**Fig. 3** Indigenously developed high-speed slurry erosion test rig: (a) schematic; (b) interaction of specimens with erodent media**Table 6** Selected ranges of investigating parameters

Parameters	Values
Rotational speed (RS)	1000 rpm; 3000 rpm
Average particle size of erodent (APS)	300 $\mu\text{m}$ ; 500 $\mu\text{m}$
Erodent concentration (EC)	10,000 weight ppm; 30,000 weight ppm
Operating time	6 h

glued pair of the specimen was kept under the pressurized conditions in a furnace for 2 h at 180  $^{\circ}\text{C}$  and then tested in tension using a tensile test rig. The resulting value of bond strength was determined by calculating the ratio of failure load to the cross-sectional area of the test specimen. For each test coating, two replicates of bond strength tests were performed to determine the average value of bond strength.

## Results and Discussion

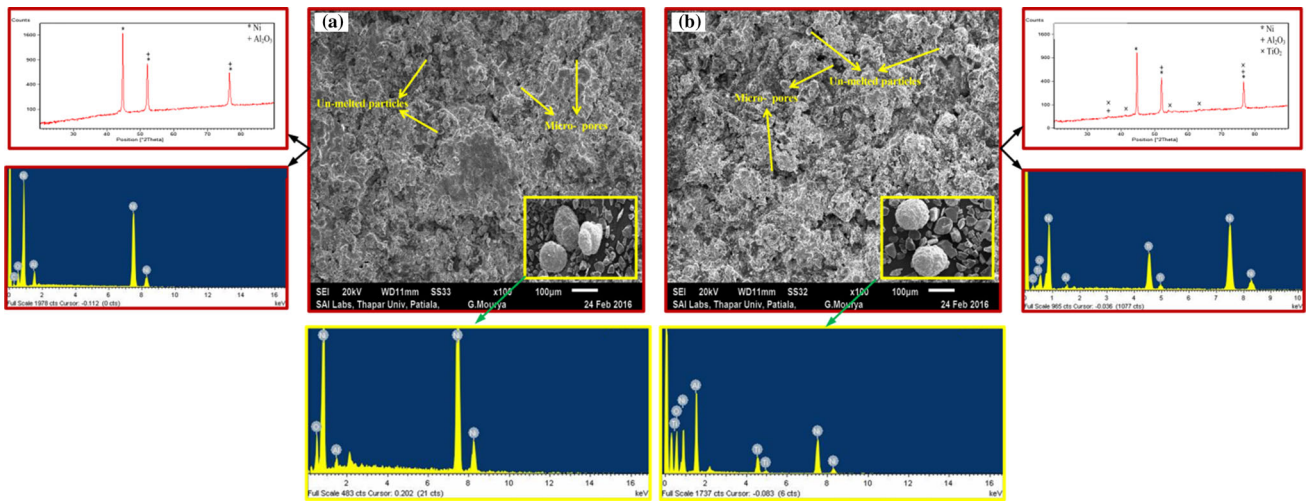
### Microstructural Characterization

Figure 4 presents the SEM micrographs along with EDS and XRD analysis of Ni-A- and Ni-AT-coated surfaces in as-sprayed conditions. Figure 4 also depicts the EDS



**Table 7** Taguchi’s L4 orthogonal array of experimental design

Various runs	Investigated parameters and their values		
	Rotational speed (RS)	Average particle size of erodent (APS)	Erodent concentration (EC)
E1	1000	300	10,000
E2	1000	500	30,000
E3	3000	500	10,000
E4	3000	300	30,000



**Fig. 4** SEM, EDS and XRD analysis of: (a) Ni-A; (b) Ni-AT coatings in as-sprayed condition

**Table 8** Observed values of surface roughness, bond strength and microhardness

Coating (condition)	Mechanical properties		
	Roughness, $R_a$ , $\mu\text{m}$	Bond strength, MPa	Microhardness (HV <sub>0.3</sub> )
Ni-20A (as-sprayed)	$3.41 \pm 0.4$	$56.16 \pm 2.9$	$576 \pm 23$
Ni-20A (eroded)	$2.52 \pm 0.3$	...	...
Ni-10A-10T (as-sprayed)	$2.95 \pm 0.3$	$63.40 \pm 3.2$	$460 \pm 16$
Ni-10A-10T (eroded)	$2.19 \pm 0.2$	...	...

analysis of feedstock powders used for fabricating the required deposits. The defects, such as unmelted particles and micropores, can be easily observed on the surface of each coating. The presence of unmelted region can have a significant detrimental impact on the mechanical properties of the coating, whereas the existence of micropores enables the erosive particles to reach easily to the substrate surface, thus affecting the erosion performance of coatings. The distinct regions, such as melted, partially melted and unmelted, can be easily accessed from the surface micrographs of both the coatings. The marginal variation in melting point temperature of various particulates might be responsible for the formation of these regions. The results of surface roughness of coatings in as-sprayed as well as in eroded conditions are presented in Table 8. In each case,

the eroded specimens are found to have a less magnitude of surface roughness than as-sprayed specimens. The smoothing done by the slurry particles during the impacts might be responsible for such behavior.

Figure 5 illustrates the cross-sectional micrographs of deposited Ni-A and Ni-AT coatings. Both the coatings seem to have defect-free interface (i.e., absence of cracks and inclusion of foreign particles), which indicates better and continuous contact between deposit and substrate material. The cross-sectional micrograph of both the coatings shows an insignificant variation in the population of number of pores. These findings are a good agreement with the results as recorded during porosity measurement ( $1.43\% \pm 0.17$  in case of Ni-A coating and  $1.32\% \pm 0.21$  for Ni-AT coating). The slightly higher value of porosity

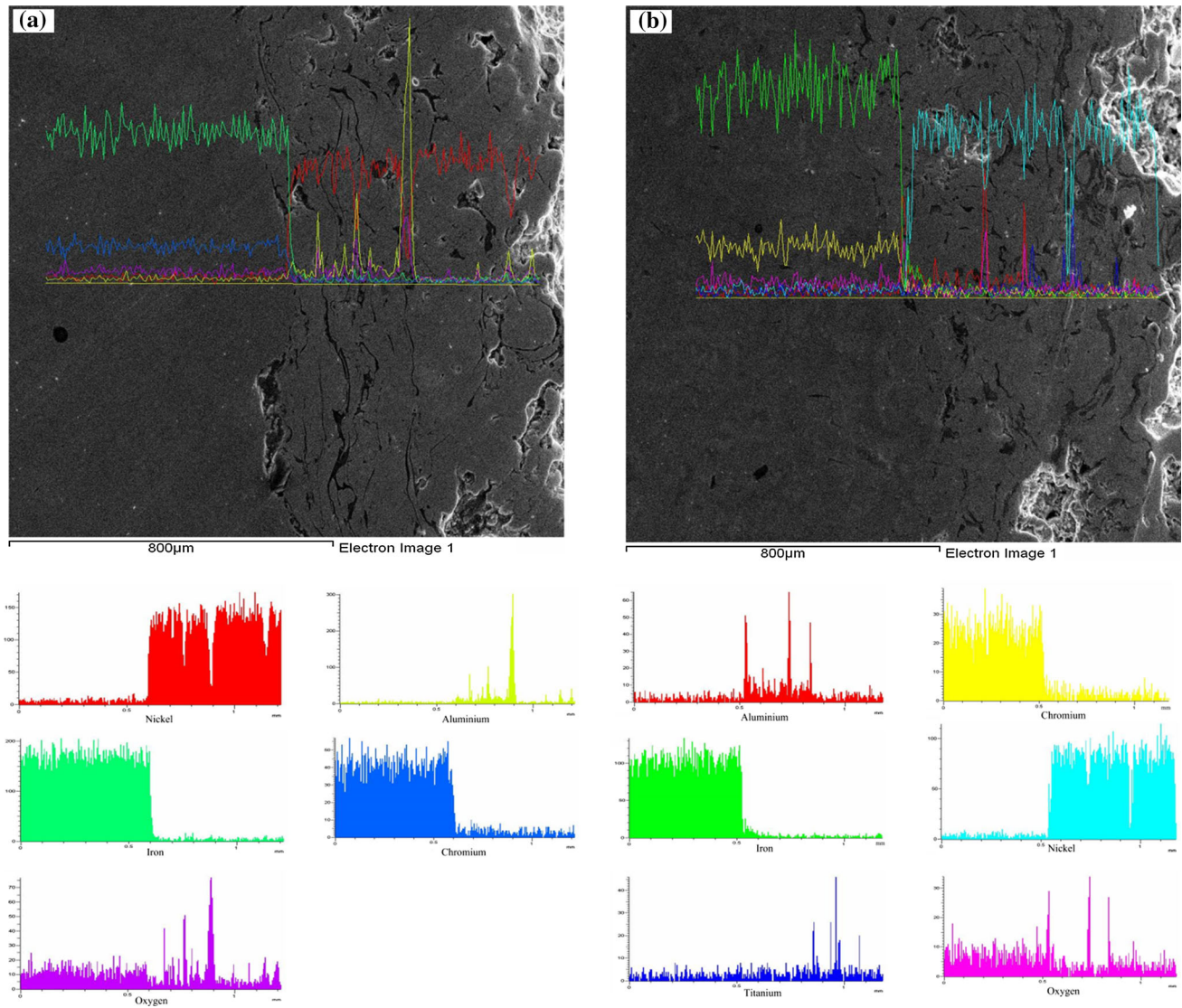


**Fig. 5** Cross-sectional analysis of: (a) Ni-A; (b) Ni-AT coatings

content in case of Ni-A coatings might be due to the presence of a comparatively higher percentage of alumina contents in Ni-A coating (20%) than in Ni-AT coating (10%). The higher melting point temperature of  $\text{Al}_2\text{O}_3$  (2040 °C) along with its higher content (20%) in Ni-A coating resulted in the generation of slightly more number of unmelted and semi-molten splats within the coating, which may further increase the porosity content within the coating. Moreover, in the case of Ni-AT coating, the particulates of Ni and  $\text{Al}_2\text{O}_3$  are found to be relatively well bonded with each other than Ni-A coating. This may be due to the presence of  $\text{TiO}_2$  particulates within the coating. As the melting temperature of  $\text{TiO}_2$  is low, it has high ability to form a liquid solution with  $\text{Al}_2\text{O}_3$ . Therefore, it can impart high adherence between the adjoining particulates (Ref 24).

### Mechanical Analysis

The results of microhardness and bond strength measurements are summarized in Table 8. Ni-A coating exhibits higher average microhardness ( $576 \pm 23 \text{ HV}_{0.3}$ ) as compared to Ni-AT coating ( $460 \pm 16 \text{ HV}_{0.3}$ ). This may be due to the presence of higher content (20%) of  $\text{Al}_2\text{O}_3$  particulates within the Ni-A coating than within the Ni-AT coating (10%). Moreover,  $\text{Al}_2\text{O}_3$  is harder than  $\text{TiO}_2$ , which again might be one of the possible reasons for such an increase in microhardness. On the other hand, the Ni-AT coating shows relatively high (11%) bond strength in comparison with Ni-A coating (Table 8). The improvement in intermetallic adhesion of the deposits with the addition of  $\text{TiO}_2$  might be the possible reason for this characteristic (Ref 24). Further, during the bond strength testing, it has



been found that the bond failure occurred at the coating-substrate interface in each case of the coating.

### Slurry Testing Results

Figure 6 demonstrates the influence of coating type on the specific mass loss ( $\text{g}/\text{m}^2$ ) and specific mass loss rate ( $\text{g}/\text{m}^2\text{h}$ ) following 6 h of slurry erosion testing. For both the coatings, the erosion rate is found to be increased with an increase in exposure time. The specific mass loss as well as specific mass loss rate analysis reveals Ni-AT-coated specimens to have exhibited comparable less erosion rate than Ni-A coatings during each set of experiments. The figure also revealed that, irrespective to the test coating, the maximum specific mass loss was observed during the experimental run 4 and minimal in the case of experimental run 1. Moreover, the plots in each case seem to be linear and no significant change in slope is observed for the complete test duration, which confirmed the absence of any wear transition throughout the test cycle. The recorded trend (Fig. 6b) indicated that the specific mass loss rate was initially high and then reduced gradually with the increase in test duration. Continuous and repeated impacts of erodent particles resulting in work hardening of the test surfaces might be attributed to such behavior. It has also been noticed from both the plots (Fig. 6a and b) that the coatings showed severe erosion during the experimental run E4 among all the experimental runs. The marginal higher values of kinetic energy and population of impacting particles during the experimental run 4 might be responsible for such response.

### Effect of Operating Parameters

Based on the observed experimental data, various plots representing the variation of specific mass loss with test parameters were prepared and are presented in Fig. 7. These plots are discussed in detail in the following sections.

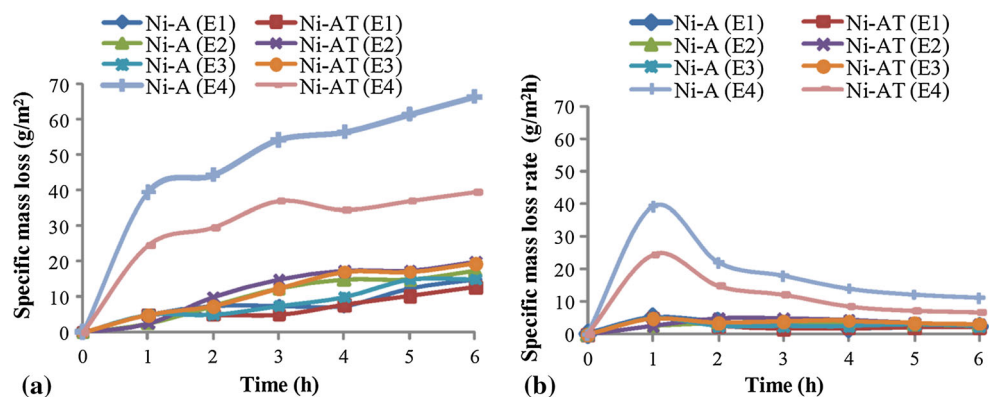
### Effect of Rotational Speed

To evaluate the effect of rotational speed/impact velocity on the specific mass loss, tests were conducted at two different levels of rotational speed (1000 and 3000 rpm). Figure 7(a) shows the variation of specific mass loss of test surfaces with rotational speed. It is evident that the specific mass loss of both the test coatings increases with the increase in rotational speed. As the process of slurry erosion takes place due to the movement of slurry particles, so it is quite expected that the slurry erosion rate will increase with the increase in rotational speed of slurry particles (Ref 3, 25-27). This may be due to the fact that, at higher rotational speeds/impact velocities, the rebounding particles are unable to effectively interact with the fresh incoming particles, as in the case of low rotational speeds. Therefore, the tendency of de-accelerated and diverted fresh incoming particles gets decreases, which may result in a higher specific mass loss. These findings are in well consistent with the previous studies (Ref 3, 26-30).

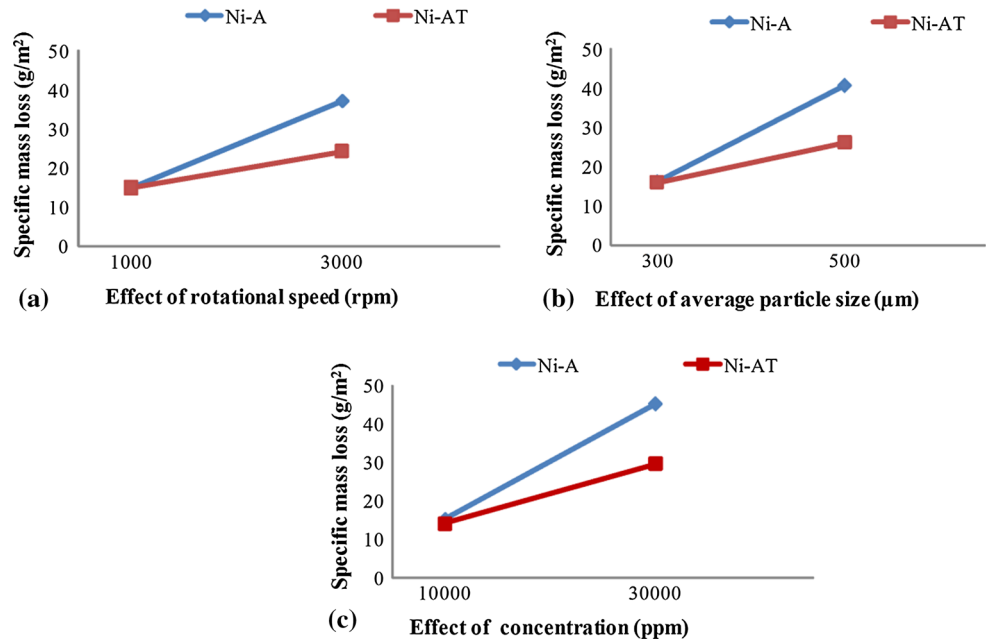
### Effect of Average Particle Size of Erodent

Figure 7(b) depicts the behavior of Ni-A and Ni-AT coatings under the effect of variation in average particle size of the erodent. The specific mass loss was found to be increased with an increase in average particle size. The increase in impact energy with the increase in erodent size might be the possible reason for such behavior (Ref 26). These results are consistent with the findings of Goyal et al. (Ref 26) and Bhandari et al. (Ref 31). Further, the value of the exponent,  $\beta$  (as determined from Eq 1), was measured to be 1.81 for Ni-A coating and 0.96 in case of Ni-AT coating, which shows that the effect of variation in average particle size of erodent is more dominating in the case of Ni-A coating rather than Ni-AT coating.

**Fig. 6** Observed trends for both the coatings at different environmental conditions: (a) specific mass loss vs. exposure time; (b) specific mass loss rate vs. exposure time



**Fig. 7** Effect of operational parameters on the erosion rate: (a) rotational speed; (b) average particle size; (c) erodent concentration



#### Effect of Erodent Concentration

The variation in specific mass loss with respect to erodent concentration, for both the test coatings, can be accessed from Fig. 7(c). It is seen that within the range of erodent concentration investigated, the specific mass loss increases with the increase in the erodent concentration. The observed trend is found to be in good agreement with the findings of Goyal et al. (Ref 26), who worked in the field of exploring the potential of CF8 M steel, WC-10Co-4Cr and  $\text{Al}_2\text{O}_3 + 13\text{TiO}_2$  coatings for different slurry environmental conditions. Moreover, the value of erodent concentration exponent,  $\gamma$  (as determined from Eq 1), was observed to be 0.94 and 0.61, respectively, for Ni-A and Ni-AT coatings. However, in each case, the reported value of erodent concentration exponent ( $\gamma$ ) is less than one. The poor collision efficiency of the impacting system may be attributed to such behavior.

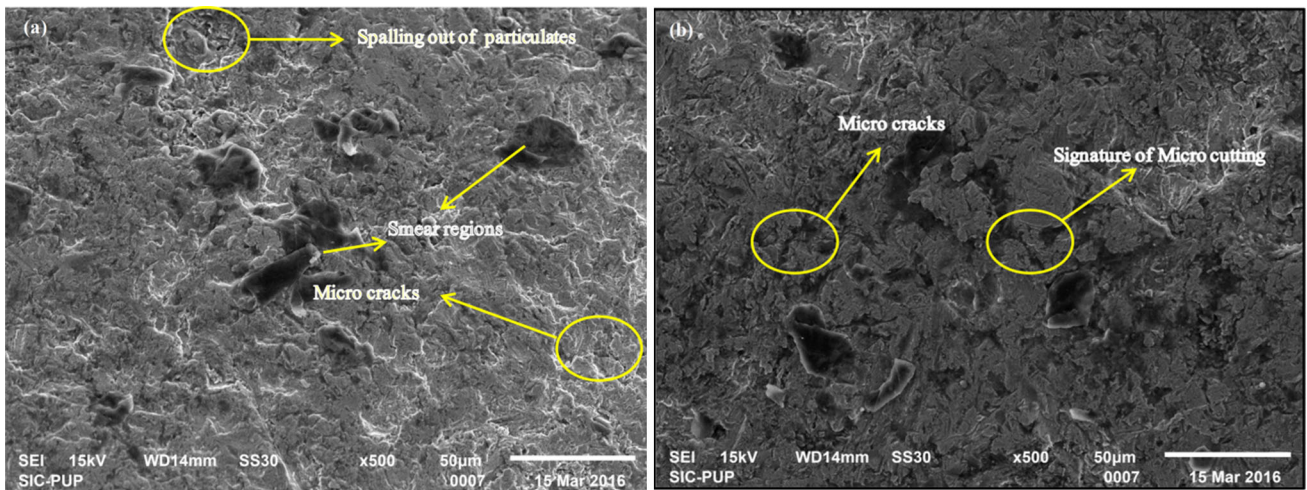
#### Examination of Eroded Surfaces

The coated specimens subjected to slurry erosion tests at various experimental conditions were examined using SEM. This facilitates further understanding and evaluation of the respective erosion mechanisms operating within the impinged region on specific coating materials. Scanning electron micrographs showing the wear scars of Ni-A and Ni-AT coatings are depicted in Fig. 8, 9, 10, and 11. Specifically, it is observed from the micrographs of impinged region of Ni-A coatings (Fig. 8a, 9a, 10a, and 11a) that the material removal takes place primarily through the brittle mode of erosion, whereas some erosion marks such as microcutting

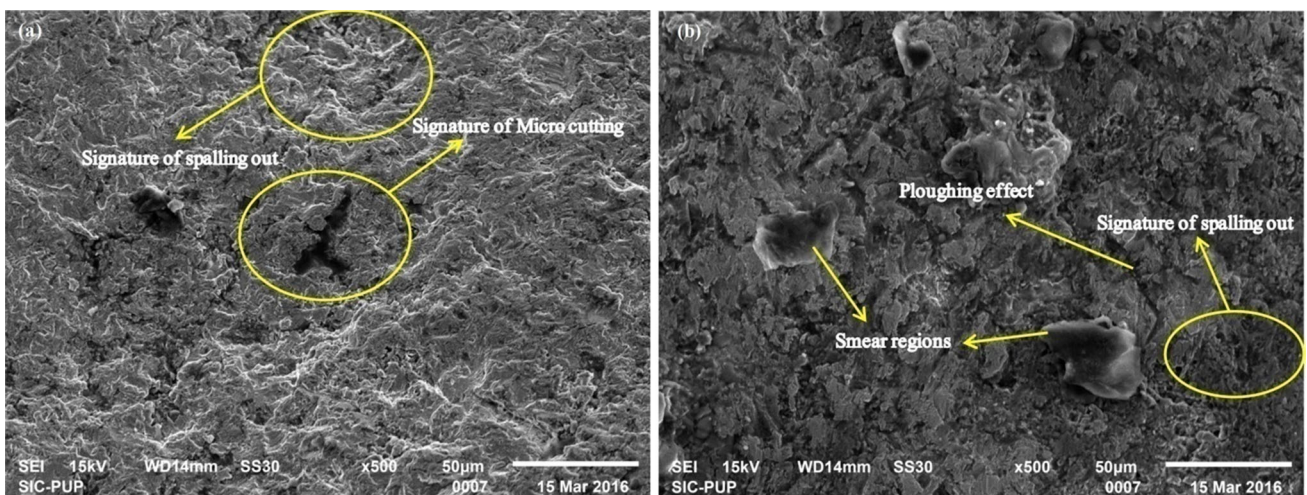
can also be seen on the eroded surfaces. The presence of Ni and  $\text{Al}_2\text{O}_3$  content within the coating might be responsible for ductile and brittle behavior, respectively. The formation of smooth craters was also observed on the eroded surface of Ni-A coatings. The formation of such craters may be due to the removal of the whole of the splat in one way or the other. Some microcracks can also be observed on the eroded surfaces, as these locations are the regions of high impact stresses. Moreover, the presence of loosely bound unmelted alumina splats (Fig. 4a) highly contributes the erosion rate of the Ni-A coatings. It appears that these splats might have been removed easily from their locations during impacts of erodent particles and thus resulted in a significant amount of material removed from the exposed surfaces. These findings are in good agreement with the observations reported by Grewal et al. (Ref 11), who evaluated the slurry erosion performance of Ni- $\text{Al}_2\text{O}_3$  coatings with varying contents of alumina particles. Evidence of scoring can be readily visible; however, it is contained within the ductile nickel phase. This feature is to be expected given the relatively low hardness of Ni over  $\text{Al}_2\text{O}_3$  particulates. Repeated impacts of erodent particles cause the failure of the ductile phase, typically initiating at the nickel-alumina interface. The removal of Ni leads to a lack of binding material capable of retaining the  $\text{Al}_2\text{O}_3$  within the coating, thus eventually resulting in them being easily plucked out from the exposed surface by the impinging erodent media. The existence of the observed signatures leads to the conclusion that the Ni-A coating demonstrates both brittle and ductile modes of material removal.

Figure 8(b), 9(b), 10(b), and 11(b) illustrate the various aspects of Ni-AT-coated eroded surfaces, as examined under





**Fig. 8** SEM micrographs of eroded: (a) Ni-A; (b) Ni-AT surfaces tested at RS 1000; APS 300; EC 10,000



**Fig. 9** SEM micrographs of eroded: (a) Ni-A; (b) Ni-AT surfaces tested at RS 1000; APS 500; EC 30,000

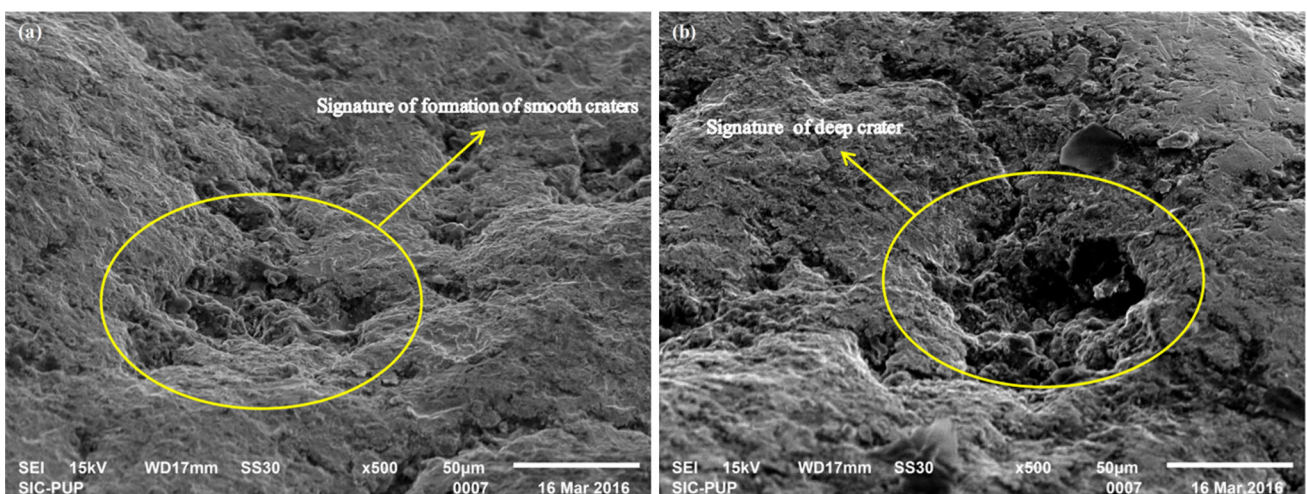


**Fig. 10** SEM micrographs of eroded: (a) Ni-A; (b) Ni-AT surfaces tested at RS 3000; APS 500; EC 10,000



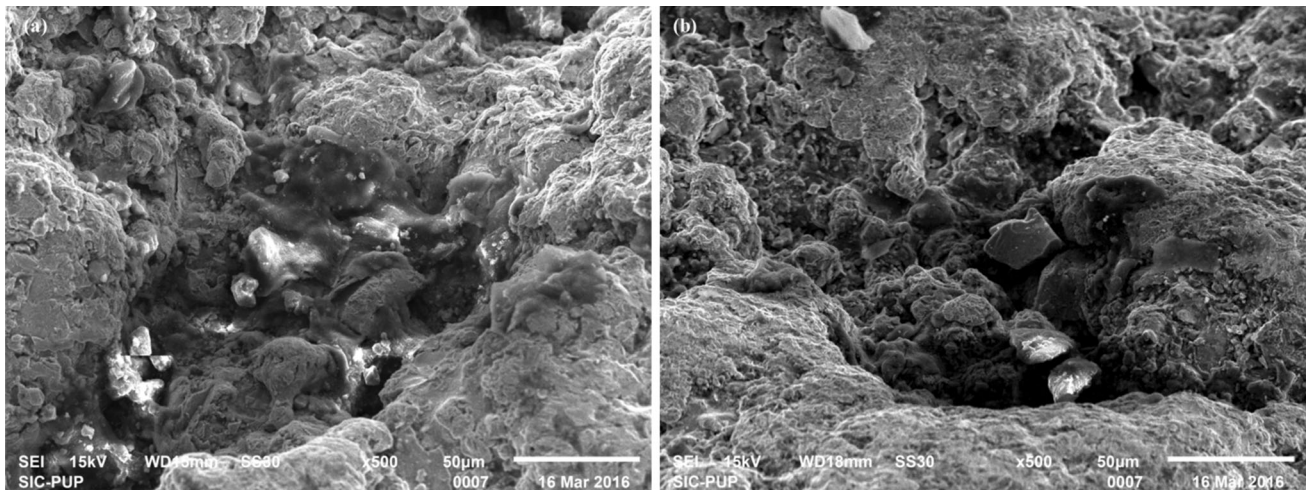


**Fig. 11** SEM micrographs of eroded: (a) Ni-A; (b) Ni-AT surfaces tested at RS 3000; APS 300; EC 30,000

SEM. The erosion spots such as cracks, microcutting and pit formation can be seen on the eroded surfaces. It may be assumed that the  $\text{Al}_2\text{O}_3$  particulates show significant erosion resistance during the initial hours of slurry erosion testing. However, after some time, these hard phases start spalling out from the matrix phase due to the continuous striking of erodent particles. During this process, the bond strength between the particulates is supposed to be playing an important role. The higher bond strength ensures a significant increase in intermetallic adhesion, which further can reduce the possibility of spalling out of the particulates. In the present case, the addition of  $\text{TiO}_2$  phase may contribute to increasing in bond strength of Ni-AT coating. The significant improvement in adhesion strength of  $\text{Al}_2\text{O}_3$  coatings with the addition of  $\text{TiO}_2$  has already been reported by Xue et al. (Ref 12). The high ability of  $\text{TiO}_2$  to form a liquid solution with  $\text{Al}_2\text{O}_3$  may be the possible reason for the improvement in adhesion strength, which further enhanced the coating performance. Additionally, the experimental results, as well as SEM micrographs observations, indicate that the slurry erosion resistance of Ni-A coatings can be significantly improved with the addition of titania.

## Conclusions

The synergistic effect of  $\text{Al}_2\text{O}_3$  and  $\text{TiO}_2$  reinforcements on the performance of Ni-based coatings was evaluated in the present work. The following conclusions can be made from this study:

- Ni- $\text{Al}_2\text{O}_3$  and Ni- $\text{Al}_2\text{O}_3$ - $\text{TiO}_2$  coatings were successfully deposited on CA6NM steel.
- The presence of  $\text{TiO}_2$  in Ni- $\text{Al}_2\text{O}_3$  coatings is a vital controlling factor that significantly controls the slurry erosion resistance.

- Irrespective of the test conditions, the Ni- $\text{Al}_2\text{O}_3$ - $\text{TiO}_2$  coating showed better results against slurry erosion resistance in comparison with the Ni- $\text{Al}_2\text{O}_3$  coating.
- Each of the slurry test parameters such as rotational speed, average particle size of erodent and erodent concentration has a proportional effect on the erosion rate of both the coatings.
- The obtained erosion marks indicate that both the coatings exhibited the mixed behavior (brittle and ductile) of material removal mechanisms during the slurry erosion testing.

## References

1. D.V. Khera and R.S. Chadhwork, Silt Erosion: Trouble for Turbines, *Int. Water Power Dam Constr.*, 2001, **53**, p 22-23
2. S.K. Singal and R. Singh, *Impact of Silt on Hydro Turbines*, International Himalayan Small Hydropower Summit, Dehradun, 2006, p 218-225
3. H.S. Grewal, A. Agrawal, and H. Singh, Slurry Erosion Mechanism of Hydroturbine Steel: Effect of Operating Parameters, *Tribol. Lett.*, 2013, **52**, p 287-303
4. M.K. Padhy and R.P. Saini, Effect of Size and Concentration of Silt Particles on Erosion of Pelton Turbine Buckets, *Energy*, 2009, **34**, p 1477-1483
5. Y. Iwabuchi and S. Sawada, *Metallurgical Characteristics of a Large Hydraulic Runner Casting of Type 13Cr-Ni Stainless Steel*, ASTM, West Conshohocken, 1982, p 332-354
6. K. Sugiyama, S. Nakahama, S. Hattori, and K. Nakano, Slurry Wear and Cavitation Erosion of Thermal-Sprayed Cermets, *Wear*, 2005, **258**(5-6), p 768-775
7. H.S. Grewal, H. Singh, A. Agrawal, and H.S. Arora, Evaluation and Development of Economically Viable Coatings for Erosion Protection of Hydroturbines, *Adv. Mater. Res.*, 2012, **585**, p 590-594
8. H.S. Grewal, S. Bhandari, and H. Singh, Parametric Study of Slurry Erosion of Hydroturbine Steels with and Without Detonation Gun Spray Coatings Using Taguchi Technique, *Metall. Mater. Trans.*, 2012, **43**(9), p 3387-3401



9. P.S. Babu, B. Basu, and G. Sundararajan, The Influence of Ero- dent Hardness on the Erosion Behavior of Detonation Sprayed WC-12Co Coatings, *Wear*, 2011, **270**, p 903-913
10. R.J.K. Wood, B.G. Mellor, and M.L. Binfield, Sand Erosion Performance of Detonation Gun Applied Tungsten Carbide/ Cobalt–Chromium Coatings, *Wear*, 1997, **211**, p 70-83
11. H.S. Grewal, A. Agrawal, and H. Singh, Slurry Erosion Perfor- mance of Ni-Al<sub>2</sub>O<sub>3</sub> Based Composite Coatings, *Tribol. Int.*, 2013, **66**(3), p 296-306
12. W.B. Xue, C. Wang, Z.W. Deng, R.Y. Chen, Y.L. Li, and T.H. Zhang, Evaluation of the Mechanical Properties of Microarc Oxidation Coatings and 2024 Aluminium Alloy Substrate, *J. Phys.: Condens. Matter*, 2002, **14**, p 10947-10952
13. C. Duan and V.I.A. Karelin, *Abrasive Erosion & Corrosion of Hydraulic Machinery*, Imperial College Press, Covent Garden, 2002
14. M.A. Al-Bukhaiti, S.M. Ahmed, F.M.F. Badran, and K.M. Emara, Effect of Impingement Angle on Slurry Erosion Beha- viour and Mechanisms of 1017 Steel and High-Chromium White Cast Iron, *Wear*, 2007, **262**, p 1187-1198
15. H.M. Clark, Particle Velocity and Size effects in Laboratory Slurry Erosion Measurements or Do you Know What Your Par- ticles are Doing?, *Tribol. Int.*, 2002, **35**, p 617-624
16. H.M. Clark, The Influence of the Flow Field in Slurry Erosion, *Wear*, 1992, **152**, p 223-240
17. R. Gupta, S.N. Singh, and V. Seshadri, Prediction of Uneven Wear in a Slurry Pipeline on the Basis of Measurements in a Pot Tester, *Wear*, 1995, **184**, p 169-178
18. B.K. Gandhi, S.N. Singh, and V. Seshadri, Study of the Para- metric Dependence of Erosion Wear for the Parallel Flow of Solid–Liquid Mixtures, *Tribol. Int.*, 1999, **32**, p 275-282
19. G.R. Desale, B.K. Gandhi, and S.C. Jain, Effect of Ero- dent Properties on Erosion Wear of Ductile Type Materials, *Wear*, 2006, **261**, p 914-921
20. H. Singh, K. Goyal, and D.K. Goyal, Experimental Investigations on Slurry Erosion Behaviour of HVOF and HVOLF Sprayed Coatings on Hydraulic Turbine Steel, *Trans. Indian Inst. Metals*, 2016, doi:10.1007/s12666-016-0956-y
21. P.N. Rao, *Manufacturing Technology*, 2nd ed., TMH Publishing Company Limited, New Delhi, 2007
22. R.W. Heine et al., *Principles of Metal Castings*, 2nd ed., TMH Publishing Company Limited, New Delhi, 1967
23. ASTM, *Standard Test Method for Adhesion or Cohesion Strength of Thermal Spray Coatings*, ASTM Standard C 633-01, ASTM International, West Conshohocken, 2001
24. S. Jia, Y. Zou, J. Xu, J. Wang, and L. Yu, Effect of TiO<sub>2</sub> Content on Properties of Al<sub>2</sub>O<sub>3</sub> Thermal Barrier Coatings by Plasma Spraying, *Trans. Nonferrous Met. Soc. China*, 2015, **25**, p 175-183
25. H. Singh, K. Goyal, and D.K. Goyal, Slurry Erosion Behaviour of Plasma Thermal Sprayed (50%) WC-Co-Cr and Ni-Cr-B-Si Coatings of Different Thickness on CA6NM Turbine Steel Material, *Manuf. Sci. Technol.*, 2014, **2**, p 81-92
26. D.K. Goyal, H. Singh, H. Kumar, and V. Sahni, Slurry Erosion Behavior of HVOF Sprayed WC-10Co-4Cr and Al<sub>2</sub>O<sub>3</sub> + 13TiO<sub>2</sub> Coatings on a Turbine Steel, *Wear*, 2012, **289**, p 46-57
27. S. Bhandari, H. Singh, H.K. Kansal, and V. Rastogi, Slurry Erosion Performance Study of Detonation Gun Sprayed WC-10Co-4Cr Coatings on CF8 M Steel Under Hydro-Accelerated Conditions, *J. Therm. Spray Technol.*, 2012, **21**, p 1054-1064
28. D.K. Goyal, H. Singh, and H. Kumar, An Overview of Slurry Erosion Control by the Application of High Velocity Oxy Fuel Sprayed Coatings, *Proc. Inst. Mech. Eng. Part J: J. Eng. Tribol.*, 2011, **225**, p 1092-1105
29. H. Singh, K. Goyal, and D.K. Goyal, Slurry Erosion Behaviour of Plasma Thermal Sprayed (50%) WC-Co-Cr and Ni-Cr-B-Si Coatings of Different Thickness on CA6NM Turbine Steel Material, *Manuf. Sci. Technol.*, 2014, **2**, p 81-92
30. G. Singh, R.L. Virdi, and K. Goyal, Experimental Investigation of Slurry Erosion Behaviour of Hard Faced AISI, 316L Stainless Steel, *Univers. J. Mech. Eng.*, 2015, **3**, p 52-56
31. S. Bhandari, H. Singh, H.K. Kansal, and V. Rastogi, Slurry Erosion Behavior of Detonation Gun Spray Al<sub>2</sub>O<sub>3</sub> and Al<sub>2</sub>O<sub>3</sub>-13TiO<sub>2</sub>-Coated CF8 M Steel Under Hydro Accelerated Condi- tions, *Tribol. Lett.*, 2012, **45**, p 319-331